Molecular Simulation of CO2 Solubility and Its Effect on Octane Swelling

ARTICLE *in* ENERGY & FUELS · MAY 2013

Impact Factor: 2.79 · DOI: 10.1021/Ef400283n

4 AUTHORS, INCLUDING:

Junfang Zhang
The Commonwealth Scientific and Industri…
33 PUBLICATIONS **285** CITATIONS
SEE PROFILE

Keyu Liu
PetroChina Company Limited
131 PUBLICATIONS **805** CITATIONS
SEE PROFILE

energy&fuels

Article

pubs.acs.org/EF

Molecular Simulation of CO_2 Solubility and Its Effect on Octane Swelling

Junfang Zhang,[†] Zhejun Pan,*[,‡] Keyu Liu,[†,§] and Nick Burke[‡]

[†]CSIRO Earth Science and Resource Engineering, 26 Dick Perry Avenue, WA 6151, Australia

[‡]CSIRO Earth Science and Resource Engineering, Private Bag 10, Clayton South, VIC 3169, Australia

[§]Research Institute of Petroleum Exploration and Development, PetroChina, Beijing 100083, China

ABSTRACT: Carbon dioxide (CO_2) flooding is one of the very important industrial processes for enhanced hydrocarbon recovery. Therefore, a better understanding of the CO_2 solubility and its effect on hydrocarbon swelling is vital for a successful CO_2 flooding project. In this study, CO_2 solubility in octane and its effect on octane (*n*-octane) swelling are investigated by performing configurational-bias Monte Carlo simulations in the osmotic ensemble at two temperatures of 323 and 353 K and a pressure range of 2−10 MPa. This study provides a quantitative understanding of the relationship between the CO_2 solubility and the octane density reduction/swelling. The simulated swelling factor of the CO_2 saturated octane is linearly correlated to the CO_2 solubility. The results are in good agreement with the linear correlation derived from the published experimental data. Our results have also indicated that the interaction between the octane and CO_2 is the main cause of the octane swelling. Molecular modeling proves to be a valuable tool for the calculation of gas solubility in the hydrocarbon and its effect on the swelling factor, and this method is applicable to a wide range of gas-oil systems.

1. INTRODUCTION

Molecular modeling has been increasingly applied in hydrocarbon and gas research to gain a better understanding of the interactions taking place at atomic and molecular levels and to investigate the structure, dynamics, and rheology of a mixture system. Under some extreme conditions, e.g., high temperatures and pressures, experiments are impractical or impossible, and molecular simulations can be successfully applied to explore the fundamental scientific issues and obtain useful information about the various properties of the system. Carbon dioxide flooding has been recognized as one of the most effective enhanced hydrocarbon recovery processes in gas/oil reservoirs. This process requires accurate simulation before implementing in the field. Carbon dioxide solubility is a crucial parameter affecting the hydrocarbon viscosity and its swelling which, in turn, enhance its mobility and relative permeability and contribute to the enhanced hydrocarbon recovery.[1−4]

Experimental studies and reservoir simulations on CO_2 and hydrocarbon mixtures[5−12] were carried out to improve hydrocarbon recovery. Pressure/volume/temperature (PVT) studies and core flood experiments indicated that the important mechanism for hydrocarbon recovery by gas injection was mainly a hydrocarbon volume increase and viscosity reduction, and pure CO_2 appeared to be the best recovery agent.[13−16] Some authors have investigated the potential of carbonated (CO_2-enriched) water injection for improving recovery from hydrocarbon reservoirs with the added benefit of safe storage of CO_2 by conducting high-pressure flow visualization, core flood experiments, and detailed compositional simulation at reservoir conditions.[17,18] In addition to time-consuming experimental methods and reservoir models, CO_2-hydrocarbon solubility parameters have been obtained from correlations available in the literature.[16,19−22] Recently, the solubility and self-diffusion of carbon dioxide and hydrogen sulfide in linear polyethylene melts and brines were reported.[23,24] Attempts to understand the thermal behavior at hydrocarbon-solid surfaces have been made using molecular modeling by a number of authors.[25−28] There has been extensive research on the effect of CO_2 dissolution on hydrocarbon viscosity, and many correlations have been developed. Density effects from dissolution have not been taken into account in the past. They are often ignored in modeling of CO_2 injection.[29−33] In the literature, there are limited data on CO_2 solubility and its effect on density change for gas-hydrocarbon systems.[34]

The molecular modeling approach can be useful for understanding hydrocarbon recovery processes taking place in the reservoir and play an important role in understanding the mechanisms of the CO_2 induced hydrocarbon swelling. To the best of our knowledge, no molecular simulations have been carried out to investigate the pressure and temperature effect on the CO_2 solubility and establish the relationship between the solubility and the swelling factor from a molecular simulation perspective. Osmotic ensemble molecular simulation methods can be used to investigate the solubility of CO_2 in hydrocarbons and the structural change of hydrocarbons upon adsorption of guest molecules. In the osmotic ensemble, the volume of the system and the number of particles of each type are allowed to fluctuate. It is a mix of the grand canonical ensemble and the isothermal−isobaric ensemble. Further details are addressed in section 2.

The purpose of this study is to calculate CO_2 solubility and its effect on hydrocarbon swelling and to establish the relationship between them by performing molecular simulations at two temperatures of 323 and 353 K, which

Received: February 18, 2013
Revised: April 5, 2013
Published: April 8, 2013

dx.doi.org/10.1021/ef400283n | *Energy Fuels* 2013, 27, 2741−2747

Table 1. Energy Terms and Parameters for United Atom Force Field of Octane[35,36]

component	parameter value	energy
harmonic bond	k_1/k_B = 96 500 [K/Å^2], r_0 = 1.54 Å	$U^{bond} = \frac{1}{2}k_1(r - r_0)^2$
harmonic bend	k_2/k_B = 62 500 [K/rad^2] θ_0 = 114°	$U^{bend} = \frac{1}{2}k_2(\theta - \theta_0)^2$
torsional potential	$c_0 = 0$ c_1/k_B = 335.03 [K] c_2/k_B = 335.03 [K] c_3/k_B = 335.03 [K]	$U^{tors} = c_0 + c_1[1 + \cos\phi] + c_2[1 - \cos(2\phi)] + c_3[1 + \cos(3\phi)]$

correspond to the injection site depths of around 1400 m and 2600 m. These depths are within the range of carbon dioxide injection depths. A pressure range of 2−10 MPa is considered. The reason why we chose the molecular simulation method is that it can offer information which cannot be obtained from experiment on grounds of cost or difficulty at extreme conditions. The systems of pure and CO_2 saturated octane are simulated. It was anticipated that the molecular modeling would assist in evaluating the effect of CO_2 on the underground hydrocarbon recovery and the environmental safety for CO_2 storage. The remainder of this paper is structured as follows. In section 2 we explain the intermolecular potentials and simulation details. In section 3 we present the results and discussions, and finally we summarize and conclude our analysis in section 4.

2. SIMULATION DETAILS

The octane molecules are described with a united atom model, the transferable potentials for phase equilibria (TraPPE) model,[35,36] in which each CH_3 and CH_2 group in octane is treated as pseudoatom, a single interaction center with their own effective potentials and the pseudoatoms are connected by harmonic C−C bond length, C−C−C bond angle, and dihedral potentials. The nonbonded interactions between pseudoatoms which are separated by more than three bonds, or belong to different molecules, are described by pair wise-additive Lennard-Jones (LJ) 12−6 potentials expressed as follows:

$$u(r_{ij}) = \begin{cases} 4\varepsilon_{ij}\left[\left(\frac{\sigma_{ij}}{r_{ij}}\right)^{12} - \left(\frac{\sigma_{ij}}{r_{ij}}\right)^{6}\right] & \text{for } (r_{ij} \le r_{cut}) \\ 0 & \text{for } (r_{ij} > r_{cut}) \end{cases} \quad (1)$$

where r_{ij}, ε_{ij}, and σ_{ij} are the separation, LJ well depth, and LJ radius, respectively, for the pair of atoms i and j. r_{cut} is the cutoff distance in the LJ potentials. Interactions longer than this distance are omitted from the energy and force computations. Cross interactions (interactions between unlike species) are calculated by the Lorentz−Berthelot mixing rules as given below

$$\sigma_{ij} = \frac{1}{2}(\sigma_{ii} + \sigma_{jj}) \quad (2)$$

$$\varepsilon_{ij} = \sqrt{\varepsilon_{ii}\varepsilon_{jj}} \quad (3)$$

The LJ parameters and energy terms and parameters for octane are taken from refs 35 and 36 and summarized in Table 1. The interactions between CO_2 molecules are modeled by LJ and Coulomb potentials. The Coulomb interactions in the system are calculated by Ewald summation for periodic systems.[37] CO_2 molecules are taken linear and rigid with a C−O bond length of 1.15 Å but with a flexible bond angle potential of $(1/2)k_\theta(\theta - \theta_0)^2$, where k_θ = 1236 kJ/mol/rad^2 according to the EPM2 model developed by Harris et al.[38] We use a truncated and shifted potential with cutoff radius of 12 Å. Structural and thermodynamic properties are obtained for pure and CO_2 saturated octane by configurational-bias Monte Carlo (CBMC)[39,40] simulations in the osmotic ensemble for a pressure range of 2−10 MPa and two temperatures of 323 and 353 K. The CBMC algorithm allows efficient numerical simulation of systems consisting of flexible chain molecules. The method is especially suitable for the numerical simulation of dense chain systems. Using this technique, a chain molecule is grown segment by segment in such a way that for the insertion of each segment several trial segments are generated and one of these trial segments is selected with a certain probability. This technique has found many applications.

In the osmotic ensemble, the number of molecules of octane is fixed, and the number of CO_2 is allowed to change according to its chemical potential imposed. Instead of setting the chemical potential, it is more intuitive to set the reservoir pressure which is related to the chemical potential by $\mu = \mu^0 + RT\ln(\phi P/p^0)$, where μ is the chemical potential, p^0 and μ^0 are the standard pressure and chemical potential, respectively. P is the reservoir pressure and ϕ is the fugacity coefficient. The temperature, T, and the chemical potential of the CO_2 phase, μ, which is assumed to be in equilibrium with a gas reservoir, are fixed. The total volume V is allowed to change when octane absorbs/desorbs gases. The osmotic ensemble allows the number of adsorbate (CO_2) to change while keeping the number of solvent (octane) molecules fixed. Simulations with the fixed number of 50 and 100 octane molecules show no size effect for the system of octane and CO_2. In the limiting case where the volume is a constant, for example, gas adsorption in a rigid frame of zeolite,[41] the osmotic ensemble is equivalent to the grand canonical (GCMC) ensemble. GCMC algorithm allows the system density to fluctuate with insertion and deletion of adsorbate molecules. Equilibrium is attained when the number of successful swap insertion and swap deletion attempts balances each other. This is necessary to obey a detailed balance. Details of the GCMC method can be found in refs 42 and 43. The simulations are carried out using the open source package RASPA 1.0 developed by Dubbeldam et al.[44] They are performed using one orthorhombic unit cell, and isotropic volume changes allow the system to reach its equilibrium value at the specified pressure. Octane molecules moved around by translation, rotation, and regrowth and the relative frequency of the three moves is given by 1:1:1. For CO_2 molecules, the Monte Carlo moves are translation, rotation, reinsertion, and swap. The relative frequency of the four moves is 1:1:1:1. The swap move is the one related to the change of the number of molecules. This move imposes a chemical equilibrium between the system and an imaginary reservoir. We applied a volume change probability of 0.35 to allow the volume of the simulation box to fluctuate in order to equilibrate the system with respect to the applied pressure. A typical production run was six million Monte Carlo steps after the system reaches equilibrium for each pressure and temperature. The number of Monte Carlo steps is roughly the number of cycles times the average number of molecules. Time step is 0.001 ps. For six million time steps, it takes around 360 h. We run MPI parallel programming with 4 processors in the SGI Altix XE Cluster in the National Computational Infrastructure (NCI) Australia to speed up the simulations. The simulation unit cell is shown in Figure 1. The evolution of the total energy and density over the Monte Carlo steps was monitored to check for the equilibration conditions. Once the system has reached equilibrium we calculated the average value of the properties we are interested. Error bars are of the order of the size of the plotting symbols and they are not shown in all the plots.

dx.doi.org/10.1021/ef400283n | Energy Fuels 2013, 27, 2741−2747

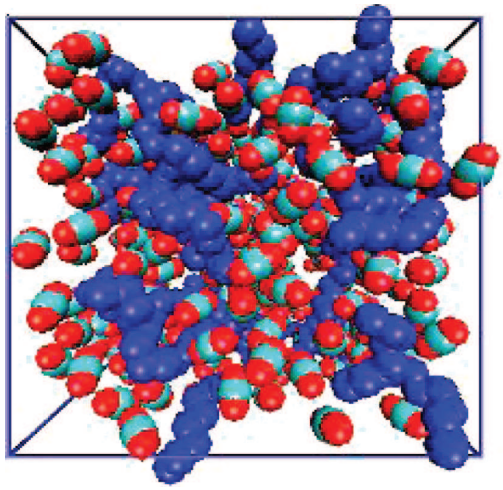

Figure 1. Simulation unit cell: dark blue chains represent octane molecules; red and light blue spheres are CO_2 molecules.

3. RESULTS AND DISCUSSION

3.1. Octane Density and CO_2 Solubility. In order to quantify the swelling of octane, we calculate the density for pure and CO_2 saturated octane as a function of pressure at a specified temperature. The results are given in Table 2 and plotted in Figure 2. The density is defined as the mass per unit volume. The density results show that the lower the temperature, the higher the density for the pure system. At 323 K, the density of the pure octane changes from 702.45 kg/m^3 to 709.17 kg/m^3 at the pressure range of 2−10 MPa. The variation of the density within the pressure range of 2−10 MPa is within 0.95%. When the temperature is increased from 323 K to 353 K, the density drops are within 3.6%. Our measured value of the density at pressure of 2 MPa and temperature of 323 K is 702.45 kg/m^3. Octane has a density of 703 kg/m^3 at the temperature of 293 K and the pressure of 1 atm. We observe that for the CO_2 saturated octane, the density decreases with increasing pressure for both temperatures. The decrease in the density of CO_2 saturated octane is due to the fact that the CO_2 solubility increases as the saturation pressure increases.[45] At the higher temperature of 353 K, the density of the CO_2 saturated octane is larger than that for the temperature of 323 K at high pressure. The reason for this can be seen by considering the CO_2 solubility as a function of pressure and temperature shown in Figures 3 and 4, and the data is listed in Table 3. It is shown that the CO_2 solubility increases with pressure but decreases with temperature. If the pressure is increased, the CO_2 molecules are forced into the octane since this will relieve the pressure that has been applied and the number of CO_2

Table 2. Measured Density of Pure and CO_2 Saturated Octane at Different Pressure and Temperature

	density of pure octane (kg/m^3)		density of CO2 saturated octane (kg/m^3)	
P (MPa)	T = 323 K	T = 353 K	T = 323 K	T = 353 K
2	702.45	677.20	643.16	647.66
4	703.48	680.62	572.57	592.22
6	704.00	683.90	502.65	544.68
8	708.20	684.00	460.03	491.09
10	709.17	685.53	411.00	447.50

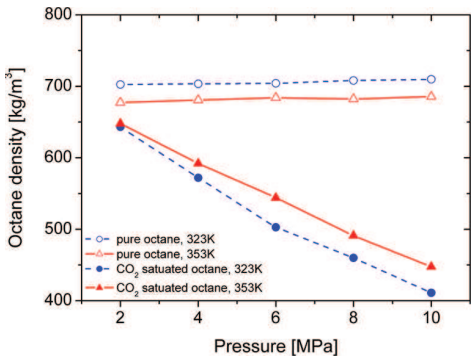

Figure 2. Density of pure and CO_2 saturated octane at different pressures and temperatures.

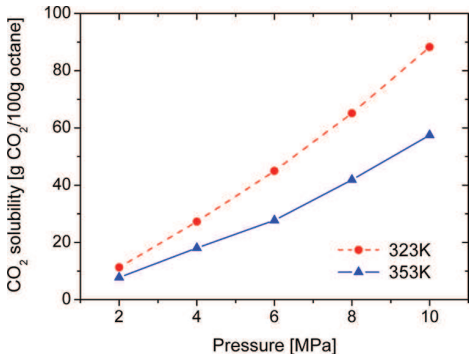

Figure 3. CO_2 solubility in the unit of g CO_2/100 g octane as a function of pressure.

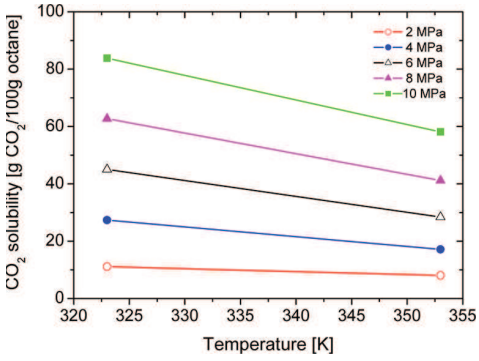

Figure 4. CO_2 solubility in the unit of g CO_2/100 g octane as a function of temperature.

Table 3. CO_2 Solubility and Swelling Factor of CO_2 Saturated Octane at Different Pressure and Temperature

	CO_2 solubility in octane (g CO_2/100g octane)		swelling factor of CO_2 saturated octane	
P (MPa)	T = 323 K	T = 353 K	T = 323 K	T = 353 K
2	11.13	6.96	1.09	1.05
4	27.36	17.11	1.23	1.15
6	47.03	28.40	1.40	1.26
8	63.26	41.85	1.53	1.39
10	86.49	58.10	1.73	1.53

dx.doi.org/10.1021/ef400283n | Energy Fuels 2013, 27, 2741−2747

molecules dissolved in octane is increased as shown in Figure 3. Henry's Law states that the solubility of a gas in a liquid is directly proportional to the partial pressure of that gas. However, increased temperature causes a decrease in the CO_2 solubility, as indicated in Table 3 and Figure 4. It is due to the fact that elevated temperature results in an increase in kinetic energy. The higher kinetic energy causes more motion in molecules which make it easy for CO_2 molecules to escape from octane. In Figure 5, the effect of CO_2 solubility and

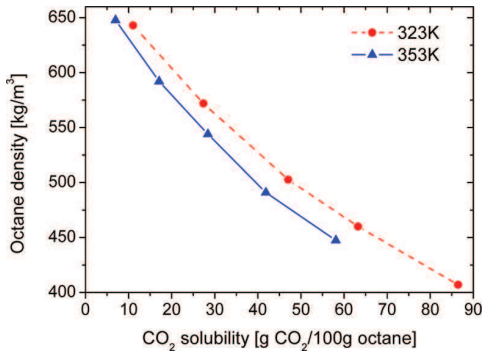

Figure 5. Effect of CO_2 solubility on the density of CO_2 saturated octane at temperatures of 323 and 353 K.

temperature on the density of CO_2 saturated octane is illustrated. For a given CO_2 solubility, the higher temperature leads to more reduction in octane density. Some authors have reported that mixtures of CO_2 and crude oil show a density increase with an increased CO_2 concentration.[34,46,47] At first glance, it seems to be in contradiction with our observations of the octane density reduction with increasing CO_2 solubility, but it should be noted that the density they measured is density of mixtures of CO_2 and crude oil. Our result is in the same trend as they have reported. In Figure 6, we show the effect of CO_2

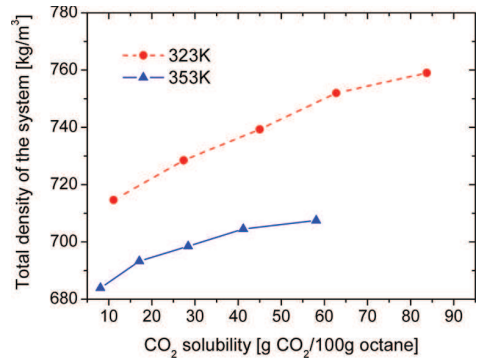

Figure 6. Effect of CO_2 solubility on the density of octane/CO_2 mixture at temperatures of 323 and 353 K.

solubility on the total density (octane plus CO_2) of the system at temperature of 323 and 353 K. The density of the mixture exhibits an increase with the CO_2 solubility. The dependence of the mixture density on the CO_2 solubility is more pronounced for the lower temperature of 323 K. In refs 46 and 48, the mole fraction of carbon dioxide dissolved in the alkanes at a temperature of 298.15 K and pressure of 1 atm was calculated from $x_{CO_2} = 0.011\,56 + (9.28 \times 10^{-6})l^2 (l > 1)$, where x_{CO_2} is the mole fraction of CO_2 and l is the carbon chain length of the alkanes. For octane, $l = 8$ and the above equation gives a value of 0.0121 for the mole fraction of CO_2 at the temperature of 298.15 K and pressure of 1 atm. We performed extra simulation for the octane/CO_2 mixture under the same temperature and pressure and obtained a CO_2 mole fraction of 0.0123, with a difference within 2% to the reported data. Our molecular modeling result is remarkably close to the experimental one, although disagreements between different determinations of gas solubility in hydrocarbons are commonly up to 10% but can exceptionally be as high as 35%.[46]

3.2. Swelling Factor. In the oil recovery research and development, the oil swelling factor is often used to quantify the oil swelling when gas dissolves into oil.[1,45,49,50] In this paper, the swelling factor is defined as the ratio of the volume of the CO_2 saturated octane divided by the volume of the pure octane under the same conditions. The measured octane swelling factors are given in Table 3 and plotted in Figure 7 as a

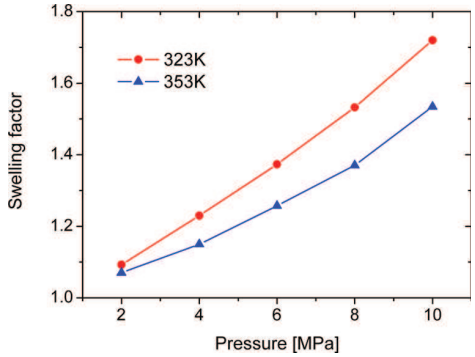

Figure 7. Swelling factor as a function of pressure.

function of pressure at two temperatures. Figure 7 clearly shows that the swelling factors of the octane increase with the pressure. This is due to the fact that the increase in the pressure leads to greater solubility of CO_2 in the octane. At the temperature of 323 K, the pressures of 2, 4, 6, 8, and 10 MPa correspond to the swelling factor of around 1.09, 1.23, 1.40, 1.53, and 1.73, respectively. Oil with an API greater than 30° is termed light; between 22° and 30°, medium; below 22°, heavy; and below 10°, extra heavy. In ref 50, oil swelling factors for the CO_2-heavy oil system are around 1.033−1.129 at the pressure range of 2−6 MPa and the temperature of 297 K. In our CO_2−octane system, the measured values of swelling factors for octane with API of around 50° are around 1.09−1.73 at the pressure range of 2−10 MPa and a temperature of 323 K. It is not surprising that we observed a higher swelling factor than the CO_2-heavy oil system as the swelling factor for light oil is higher than that of heavy oil.[51] In the literature, Welker and Dunlop[51] provided a linear correlation for calculating the swelling factor of a CO_2-saturated oil, $k_{sw} = 1.0 + 0.0105\chi$, where χ is the solubility of CO_2 in oil (g CO_2/100 g oil). We plot the prediction of the linear correlation for the swelling factor by Welker and Dunlop[50,51] with our results of the swelling factor as a function of the CO_2 solubility in Figure 8. We found the simulated swelling factor is linearly proportional to the CO_2 solubility. At a given CO_2 solubility, the higher temperature corresponds to a higher swelling factor due to the thermal expansion, but at low solubility, the temperature effect is negligible. Both the predictions from the linear correlation of Welker and Dunlop and our simulations show that the rather

dx.doi.org/10.1021/ef400283n | Energy Fuels 2013, 27, 2741−2747

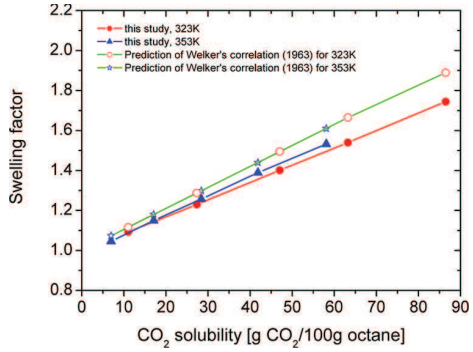

Figure 8. Swelling factor as a function of CO_2 solubility.

high solubility of CO_2 results in the high swelling. The swelling of the hydrocarbon due to the presence of dissolved CO_2 can be accurately predicted from the CO_2 solubility. Our result is in fairly good agreement with the prediction from the linear correlation derived from published experimental data within an error of 8%. It should be noted that the linear correlation between the swelling factor and CO_2 solubility, $k_{sw} = 1.0 + 0.0105\chi$, derived from experimental data does not take into account the temperature effect.

3.3. Interaction Energy. The interaction energy between octane and CO_2 as a function of pressure is presented in Figure 9. The results show that the interaction energy becomes

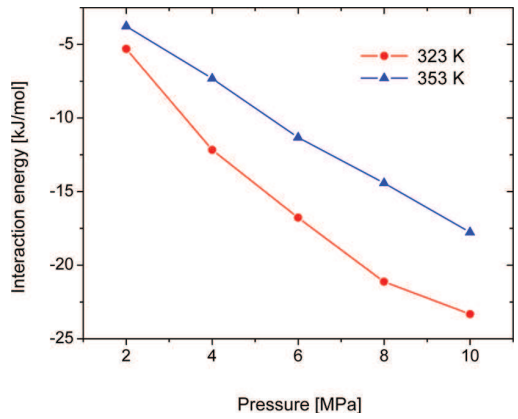

Figure 9. Interaction energy in the unit of kJ/mol of octane molecule between the CO_2 and octane as a function of pressure.

systematically more negative with increasing pressure. At a temperature of 323 K, the pressure points of 2, 4, 6, 8, and 10 MPa correspond to the interaction energies of −5.3, −12.16, −16.77, −21.11, and −23.33 kJ/mol of octane molecule, and at the temperature of 353 K, corresponding interaction energies are −3.8, −7.3, −11.3, −14.4, and −17.8 kJ/mol of octane molecules. The increasingly negative energies signify more favorable interactions between CO_2 and octane as more CO_2 molecules are dissolved into the octane. For a given pressure, the higher temperature results in the less negative interaction energy since the CO_2 solubility decreases with increasing temperature and fewer CO_2 molecules are dissolved into the octane. Therefore, the interaction between the octane and CO_2 is relatively weaker.

In order to understand the mechanism of octane swelling, we analyzed the interaction energy between CO_2−CO_2, octane−CO_2, and octane−octane and the results are presented in Figure 10. As it is shown, at low pressure, when CO_2 solubility

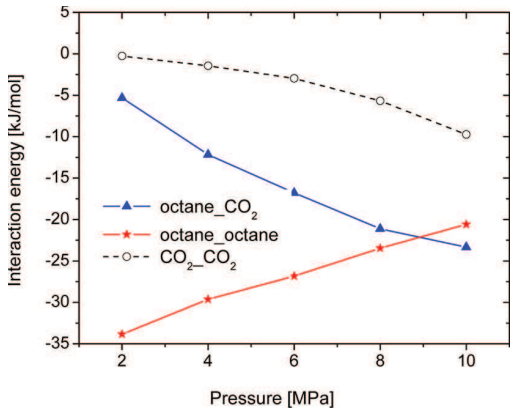

Figure 10. Comparison of the interaction energy of octane−CO_2, octane−octane, and CO_2−CO_2 in the unit of kJ/mol of octane at 323 K.

is small, the interaction between octane and octane dominates and it becomes less negative with increasing pressure. However, interaction energy between the octane and CO_2 is becoming more negative as the pressure increases indicating that the interaction between the octane and CO_2 plays an important role in the CO_2 solubility and consequent octane swelling. Although the CO_2−CO_2 interaction increases with pressure, its contribution to the total interaction energy is less than 18%. We infer that the octane swelling and the increase in the mixture density is mainly caused by strong intermolecular interactions between octane and CO_2.

3.4. Radial Distribution Functions. The radial distribution function (RDF), also called pair correlation function, is an important tool used to extract the structural information from numerical simulations. RDFs are defined as the probability that two centers, A and B, are separated by a distance r. From the RDFs, it is possible to acquire knowledge of the system density by counting the appearance of other molecules at separation r from a given molecule. To calculate the RDFs from a simulation, the neighbors around each atom or molecule are sorted into distance bins. The number of neighbors for every atom or molecule in each bin is averaged over the entire simulation. Figure 11 shows the RDFs, between the CH_3 groups in octane at the specified pressures. For clarity, we only present the results for the pressure of 2, 6, and 10 MPa. At

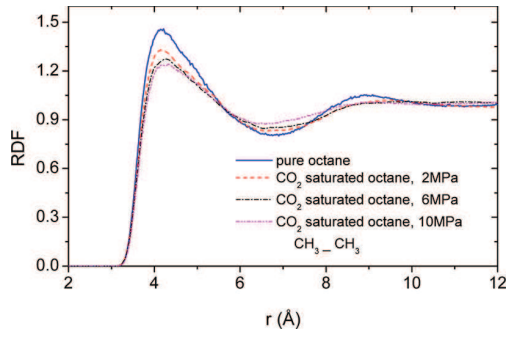

Figure 11. RDFs between the CH_3 groups in octane at the pressures specified.

dx.doi.org/10.1021/ef400283n | Energy Fuels 2013, 27, 2741−2747

short distances, RDFs is zero. This is due to the strong repulsive forces. The first and large peak occurs at $r \approx 4.15$ Å, with a value of about 1.46 for the pure octane system. This means that it is 1.46 times more likely that two CH_3 groups would be found at this separation. The radial distribution function then falls and passes through a minimum value around $r \approx 6.87$ Å. The second peak appears around $r \approx 8.95$ Å. At long distances, RDFs approach one which indicates there is no long-range order. Compared with the pure system, for the system with CO_2, both the first and second peaks become less pronounced, while the minimum increases with the increasing pressure indicating that the system becomes less structured. The RDFs for between the CH_2 groups in octane at the specified pressure are plotted in Figure 12. The close contact

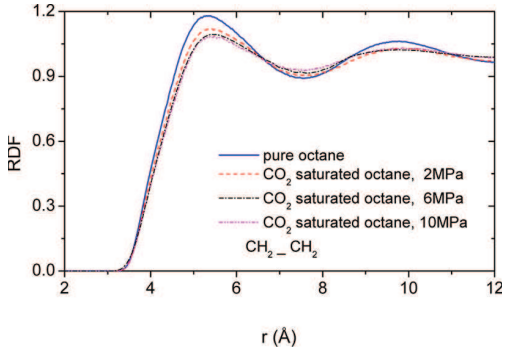

Figure 12. RDFs between the CH_2 groups in octane at the pressures specified.

peak between the CH_2 groups in octane is observed at around 5.3 Å. We observe the same trend as that shown in Figure 11. The effect of the carbon dioxide on the RDFs is that both the first peak and the second peak drop while the minimum rises with increasing pressure due to the high solubility of CO_2 in octane and the high swelling. To investigate the temperature effect on the structure of the system, the RDFs between CH_3 groups in octane and carbon in CO_2 molecules at two different temperatures are plotted in Figure 13. The temperature effect

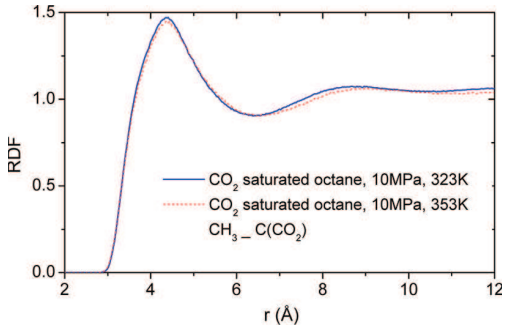

Figure 13. Temperature effect on RDFs between the CH_3 groups in octane and the carbon in CO_2 at the pressure specified.

on the RDFs is observed. Compared with the lower temperature, both the first and second peaks in the RDFs for the higher temperature decrease as a lower amount of CO_2 is dissolved. This observation agrees with the results of pressure and temperature effects on CO_2 solubility shown in Figures 3 and 4.

4. CONCLUSIONS

We have performed molecular simulations of the CO_2/octane mixture at a pressure range of 2 − 10 MPa and at temperatures of 323 and 353 K. Our results indicate that the swelling effect of CO_2 on the octane increases with the increasing solubility of CO_2. The pressure effect on the density of pure octane is negligible as the density variation is within 0.95% over the pressure range of 2−10 MPa. When the temperature increases from 323 K to 353 K, the density of the pure octane decreases by around 3%. Furthermore, the solubility of CO_2 increases with pressure. For a temperature of 323 K and a pressure of 2 MPa, the solubility of CO_2 is 11.13; it increases to 86.49 at 10 MPa. The simulated swelling factor of octane is linearly correlated to the CO_2 solubility. It is in good agreement with the linear correlation derived from the published experimental data. This study provides a quantitative understanding of the solubility of CO_2 and its swelling effect on octane. From the interaction energy results, we observe that the interaction between the octane and the CO_2 increases with an increasing amount of CO_2 dissolved. We infer that the interaction between the octane and the CO_2 is the main cause of octane swelling. Our results of the octane density, CO_2 solubility, interaction energy, swelling factor, and the RDFs are self-consistent. Molecular simulation provides quantitative solubility and swelling predictions for CO_2−octane mixtures. This method can be applied to gas and heavy oil systems. It also offers insight into aspects of the carbon dioxide storage in depleted oil fields.

AUTHOR INFORMATION

Corresponding Author

*E-mail: zhejun.pan@csiro.au.

Notes

The authors declare no competing financial interest.

ACKNOWLEDGMENTS

The authors thank the National Computational Infrastructure (NCI) national facility for a generous allocation of computing time and technical support during the course of this work.

REFERENCES

(1) Jha, K. N. *J. Can. Pet. Technol.* **1986**, *25*, 54.
(2) Do, H. D.; Pinczewski, W. V. *Chem. Eng. Sci.* **1991**, *46*, 1259.
(3) Do, H. D.; Pinczewski, W. V. *Chem. Eng. Sci.* **1993**, *48*, 3243.
(4) Orr, F. M.; Taber, J. J. *Science* **1984**, *224*, 563.
(5) Dong, M. Z.; Huang, S.; Dyer, S. B.; Mourits, F. M. *J. Pet. Sci. Eng.* **2001**, *31*, 13.
(6) Emadi, A.; Sohrabi, M.; Jamiolahmady, M.; Ireland, S.; Robertson, G. *Chem. Eng. Res. Des.* **2011**, *89*, 1783.
(7) Su, B. Y.; Fujimitsu, Y. *Energy Explor. Exploit.* **2011**, *29*, 797.
(8) Emera, M. K.; Sarma, H. K. *J. Can. Pet. Technol.* **2008**, *47*, 52.
(9) Emera, M. K.; Sarma, H. K. *Energy Sources, Part A: Recovery Util. Environ. Effects* **2007**, *29*, 1233.
(10) Mulliken, C. A.; Sandler, S. I. *Ind. Eng. Chem. Process Des. Dev.* **1980**, *19*, 709.
(11) Yang, Z. H.; Li, M. Y.; Peng, B.; Lin, M. Q.; Dong, Z. X. *J. Chem. Eng. Data* **2012**, *57*, 1305.
(12) Yang, Z. H.; Li, M. Y.; Peng, B.; Lin, M. Q.; Dong, Z. X. *J. Chem. Eng. Data* **2012**, *57*, 882.
(13) Srivastava, R. K.; Huang, S. S.; Mourits, F. M. *J. Can. Pet. Technol.* **1997**, *36*, 33.
(14) Srivastava, R. K.; Huang, S. S.; Dong, M. Z. *SPE Reservoir Eval. Eng.* **1999**, *2*, 238.
(15) Simon, R.; Graue, D. J. *J. Pet. Technol.* **1965**, *17*, 102.

(16) Simon, R.; Graue, D. J. *J. Pet. Technol.* **1964**, *16*, 1028.
(17) Sohrabi, M.; Kechut, N. I.; Riazi, M.; Jamiolahmady, M.; Ireland, S.; Robertson, G. *Chem. Eng. Res. Des.* **2011**, *89*, 1865.
(18) Sohrabi, M.; Kechut, N. I.; Riazi, M.; Jamiolahmady, M.; Ireland, S.; Robertson, G. *Transp. Porous Media* **2012**, *91*, 101.
(19) Lange, E. A. *SPE Reservoir Eval. Eng.* **1998**, *1*, 127.
(20) Emera, M. K.; Sarma, H. K. *J. Can. Pet. Technol.* **2007**, *46*, 19.
(21) Emera, M. K.; Sarma, H. K. *SPE Reservoir Eval. Eng.* **2006**, *9*, 366.
(22) Emera, M. K.; Sarma, H. K. *J. Pet. Sci. Eng.* **2005**, *46*, 37.
(23) Portier, S.; Rochelle, C. *Chem. Geol.* **2005**, *217*, 187.
(24) Faure, F.; Rousseau, B.; Lachet, V.; Ungerer, P. *Fluid Phase Equilib.* **2007**, *261*, 168.
(25) Connolly, A. J.; Roth, M. W.; Gray, P. A.; Wexler, C. *Langmuir* **2008**, *24*, 3228.
(26) Peters, G. H.; Tildesley, D. J. *Langmuir* **1996**, *12*, 1557.
(27) Roth, M. W.; Pint, C. L.; Wexler, C. *Phys. Rev. B* **2005**, 71.
(28) Pint, C. L.; Roth, M. W.; Wexler, C. *Phys. Rev. B* **2006**, 73.
(29) Hoteit, H.; Firoozabadi, A. *SPE J.* **2009**, *14*, 323.
(30) Cardenas, R. L.; Alston, R. B.; Nute, A. J.; Kokolis, G. P. *J. Pet. Technol.* **1984**, *36*, 111.
(31) Palmer, F. S.; Nute, A. J.; Peterson, R. L. *J. Pet. Technol.* **1984**, *36*, 101.
(32) Bangia, V. K.; Yau, F. F.; Hendricks, G. R. *SPE Reservoir Eng.* **1993**, *8*, 261.
(33) Jadhawar, P. S.; Sarma, H. K. *J. Can. Pet. Technol.* **2010**, *49*, 64.
(34) Ahmed, T.; Nasrabadi, H.; Firoozabadi, A. *Energy Fuels* **2012**, *26*, 4590.
(35) Martin, M. G.; Siepmann, J. I. *J. Phys. Chem. B* **1998**, *102*, 2569.
(36) Martin, M. G.; Siepmann, J. I. *J. Phys. Chem. B* **1999**, *103*, 4508.
(37) Denayer, J. F. *Ind. Eng. Chem. Res.* **1998**, *37*, 3691.
(38) Harris, J. G.; Yung, K. H. *J. Phys. Chem.* **1995**, *99*, 12021.
(39) Siepmann, J. I.; Frenkel, D. *Mol. Phys.* **1992**, *75*, 59.
(40) Frenkel, D.; Mooij, G. C. A. M.; Smit, B. *J. Phys.: Condens. Matter* **1992**, *4*, 3053.
(41) Zhang, J.; Burke, N.; Yang, Y. *J. Phys. Chem. C* **2012**, *116*, 9666.
(42) Dubbeldam, D.; Calero, S.; Vlugt, T. J. H.; Krishna, R.; Maesen, T. L. M.; Smit, B. *J. Phys. Chem. B* **2004**, *108*, 12301.
(43) Dubbeldam, D.; Calero, S.; Vlugt, T. J. H.; Krishna, R.; Maesen, T. L. M.; Beerdsen, E.; Smit, B. *Phys. Rev. Lett.* **2004**, 93.
(44) Dubbeldam, D. ; Calero, S.; Ellis, D.; Snurr, R. *RASPA, 1.0: Molecular Software Package for Adsorption and Diffusion in Nanoporous Materials*; Northwestern University: Evanston, IL, 2008.
(45) Nguyen, T. A.; Ali, S. M. F. *J. Can. Pet. Technol.* **1998**, *37*, 24.
(46) Ashcroft, S. J.; BenIsa, M. *J. Chem. Eng. Data* **1997**, *42*, 1244.
(47) Lansangan, R. M. *SPE Reservoir Eng.* **1993**, *8*, 175.
(48) Fogg, P. G. T.; Gerrard, W. *Solubility of Gases in Liquids*; Wiley: Chichester, U.K., 1991.
(49) Yang, C. D.; Gu, Y. G. *Fluid Phase Equilib.* **2006**, *243*, 64.
(50) Yang, C. D.; Gu, Y. A. *Ind. Eng. Chem. Res.* **2005**, *44*, 4474.
(51) Welker, J. R.; Dunlop, D. D. *Trans. Soc. Pet. Eng. AIME* **1963**, *228*, 873.